Clustering mechanism of oxocarboxylic acids involving hydration reaction: Implications for the atmospheric models

Ling Liu, Oona Kupiainen-Määttä, Haijie Zhang, Hao Li, Jie Zhong, Theo Kurtén, Hanna Vehkamäki, Shaowen Zhang, Yunhong Zhang, Maofa Ge, Xiuhui Zhang, and Zesheng Li

Citation: The Journal of Chemical Physics **148**, 214303 (2018); doi: 10.1063/1.5030665
View online: https://doi.org/10.1063/1.5030665
View Table of Contents: http://aip.scitation.org/toc/jcp/148/21
Published by the American Institute of Physics

Clustering mechanism of oxocarboxylic acids involving hydration reaction: Implications for the atmospheric models

Ling Liu,[1] Oona Kupiainen-Määttä,[2] Haijie Zhang,[1] Hao Li,[1] Jie Zhong,[3] Theo Kurtén,[4] Hanna Vehkamäki,[2] Shaowen Zhang,[1] Yunhong Zhang,[1] Maofa Ge,[5] Xiuhui Zhang,[1,a)] and Zesheng Li[1,b)]

[1]*Key Laboratory of Cluster Science, Ministry of Education of China, School of Chemistry and Chemical Engineering, Beijing Institute of Technology, Beijing 100081, China*
[2]*Institute for Atmospheric and Earth System Research/Physics, University of Helsinki, P.O. Box 64 (Gustaf Hällströmin katu 2a), FI-00014 Helsinki, Finland*
[3]*Department of Chemistry, University of Nebraska-Lincoln, Lincoln, Nebraska 68588, USA*
[4]*Institute for Atmospheric and Earth System Research/Chemistry, University of Helsinki, P.O. Box 64 (Gustaf Hällströmin katu 2a), FI-00014 Helsinki, Finland*
[5]*Beijing National Laboratory for Molecular Sciences (BNLMS), State Key Laboratory for Structural Chemistry of Unstable and Stable Species, Institute of Chemistry, Chinese Academy of Sciences, Beijing 100190, China*

(Received 23 March 2018; accepted 14 May 2018; published online 5 June 2018)

The formation of atmospheric aerosol particles from condensable gases is a dominant source of particulate matter in the boundary layer, but the mechanism is still ambiguous. During the clustering process, precursors with different reactivities can induce various chemical reactions in addition to the formation of hydrogen bonds. However, the clustering mechanism involving chemical reactions is rarely considered in most of the nucleation process models. Oxocarboxylic acids are common compositions of secondary organic aerosol, but the role of oxocarboxylic acids in secondary organic aerosol formation is still not fully understood. In this paper, glyoxylic acid, the simplest and the most abundant atmospheric oxocarboxylic acid, has been selected as a representative example of oxocarboxylic acids in order to study the clustering mechanism involving hydration reactions using density functional theory combined with the Atmospheric Clusters Dynamic Code. The hydration reaction of glyoxylic acid can occur either in the gas phase or during the clustering process. Under atmospheric conditions, the total conversion ratio of glyoxylic acid to its hydration reaction product (2,2-dihydroxyacetic acid) in both gas phase and clusters can be up to 85%, and the product can further participate in the clustering process. The differences in cluster structures and properties induced by the hydration reaction lead to significant differences in cluster formation rates and pathways at relatively low temperatures. *Published by AIP Publishing.* https://doi.org/10.1063/1.5030665

I. INTRODUCTION

Atmospheric aerosols have significant impacts on climate, weather, and human health.[1,2] However, the formation mechanisms and composition of atmospheric aerosols are still not fully understood, and this constitutes one of the largest uncertainties in current atmospheric models.[3,4] There is compelling evidence that sulfuric acid (**SA**), water (**W**), ammonia (**A**), or amines can play key roles in atmospheric new particle formation (NPF), but these compounds are still not efficient enough to explain NPF in all the environments where it has been observed. Recently, numerous atmospheric observations and theoretical studies have shown that organic acids can also enhance NPF.[5–15] However, there are potentially tens of thousands of different atmospheric organic species with varying properties, which makes the exact chemical composition of clusters containing organic molecules highly speculative. Furthermore, different organics have different chemical reactivities. Thus, NPF may be driven not only by clustering processes but also by various other complex and condition-dependent atmospheric chemical reactions,[16–23] which can influence the physical and chemical processes of NPF.[24–26] This makes the assessment of the role of organic compounds in the NPF process very complicated.

Oxocarboxylic acids are one of the most common organic species group found in secondary organic aerosols (SOAs) in diverse environments. Experimental and theoretical studies have shown that the equilibrium reaction between carbonyl groups and the corresponding geminal diols can occur in the gas phase,[27–30] indicating that the gas-phase hydration reaction of oxocarboxylic acids may potentially occur along with the clustering process driving NPF. As the water concentration in the atmosphere is typically 8–10 orders of magnitude higher than that of other condensing species,[31] such hydration reactions are potentially of great significance. However, in most present atmospheric aerosol formation models, the hydration reactions of oxocarboxylic acids have been neglected due to the lack of information on them. This may contribute to the discrepancy between the measured and modeled results.[3,4] In this study, we seek to understand the kinetics

a)Electronic mail: zhangxiuhui@bit.edu.cn
b)Electronic mail: zeshengli@bit.edu.cn

of atmospheric clustering processes involving hydration reactions of oxocarboxylic acids under different atmospheric environments (different precursor concentrations, relative humidities (RHs), and temperatures).

Experiments show that the gas-phase hydration reaction of glyoxylic acid (**GA**), the simplest and the most abundant oxocarboxylic acid in the atmosphere,[32,33] is able to form its geminal diol (**GW**).[27] Our previous theoretical study has also shown that this process can be effectively catalyzed by different catalysts (**SA**, **W**, or **A**), among which **SA** is the most effective, lowering the activation free energy barrier from 38.56 to 9.48 kcal/mol.[34] Therefore, **GA** has been selected as a representative example of oxocarboxylic acids in order to study the clustering mechanism involving hydration reactions. A combination of density functional theory and the Atmospheric Clusters Dynamic Code (ACDC)[35] has been used. As the hydrated clusters play an important role in cluster formation and growth,[36] water (**W**)-containing clusters are included in our study. The studied system is $(\mathbf{GA/GW})_x \cdot (\mathbf{SA})_y \cdot \mathbf{A}_z \cdot \mathbf{W}_{0-n}$, where x is the number of **GA/GW** molecules in the cluster, y is the number of **SA** molecules in the cluster, z is the number of **A** molecules in the clusters, $x + y \geq z$ (i.e., only clusters that are acidic or chemically neutral are studied), and $1 \leq x + y + z \leq 3$ (i.e., the studied clusters contain at most three molecules other than water). The maximum number of water molecules in the cluster, n, depends on the cluster type and has been chosen so that all hydrates with relative abundance higher than 5% have been included. There is always maximally one **GA** or **GW** molecule in the cluster.

II. COMPUTATIONAL METHODS

A. Quantum chemical calculations

The initial guesses for all the structures of clusters were generated by the ABCluster[37,38] program which searches for global and local minima of molecular clusters using the artificial bee colony (ABC) algorithm. In ABCluster, water molecules were described by the Transferable Intermolecular Potential with 4 Points (TIP4P) model and other molecules were described by the Chemistry at HARvard Macromolecular Mechanics 36 (ChARMM36) force field.[39] First, about 1000 structures (for each cluster stoichiometry) were generated with ABCluster, and then, these structures were optimized using the semiempirical method of PM7[40,41] using Molecular Orbital PACKage 2016 (MOPAC2016).[42] Second, up to 100 structures with relatively low energies were selected for subsequent optimization with the M06-2X[43,44] density functional and a 6-31+G* basis set. Third, the 10 best of the resulting structures were further re-optimized by the M06-2X density functional with a 6-311++G(3df,3pd) basis set.[45] The M06-2X functional is one of the most successful functionals in describing noncovalent interactions,[43] and it has been successfully used to model the thermochemistry and equilibrium structures of atmospheric clusters.[46,47] The 6-311++G(3df,3pd) basis set was chosen based on its common use for atmospherically relevant clusters[48–51] and its excellent performance to estimate cluster properties when used in conjunction with the M06-2X functional.[46] We checked that the stable structures had positive vibrational frequencies. All the quantum chemistry calculations were performed using the Gaussian 09 program package.[52]

In addition, topological analysis was performed using atoms in molecules (AIM) theory with the Multiwfn package[53] to study the nature of hydrogen bonds. The wavefunctions (technically, electron densities) computed at the M06-2X/6-311++G(3df,3pd) level of theory were used to calculate the electron density ρ and Laplacian $\nabla^2\rho$ at the bond critical points (BCPs).

B. Atmospheric cluster dynamics code (ACDC) kinetic model

The hydration reaction and clustering process of glyoxylic acids may coexist and compete against each other in the real atmosphere environment. Thus, it is necessary for cluster kinetic models to take into account the relevant chemical reactions to fully simulate the real NPF process in the atmosphere. The structural, thermodynamic, and kinetic data generated by quantum chemistry calculations were used as input in cluster formation simulations performed using the Atmospheric Cluster Dynamics Code (ACDC).[35,54]

The time development of the concentrations of each cluster was solved by integrating numerically the birth-death equations[35] using the ode15s solver in the MATLAB-R2013a program.[55] The birth-death equations can be written as

$$\frac{dc_i}{dt} = \frac{1}{2}\sum_{j<i}\beta_{j,(i-j)}c_j c_{(i-j)} + \sum_j \gamma_{(i+j)\to i}c_{i+j} - \sum_j \beta_{i,j}c_i c_j - \frac{1}{2}\sum_{j<i}\gamma_{i\to j}c_i + \sum_j k_{j\to i}c_j - \sum_j k_{i\to j}c_i + Q_i - S_i, \quad (1)$$

where c_i is the concentration of cluster i, $\beta_{i,j}$ is the collision coefficient between clusters i and j, $\gamma_{i\to j}$ is the evaporation coefficient of a molecule or a smaller cluster j from cluster i, Q_i is an outside source term of cluster i, and S_i is another possible sink term of cluster i. The coagulation sink coefficient corresponding to coagulation onto pre-existing larger particles was varied in the range of 10^{-3} s^{-1}–5×10^{-3} s^{-1}, and the results indicate that our conclusions were not influenced by these variations.[56,57] Thus, a coagulation sink coefficient of 2.6×10^{-3} s^{-1} was used for all clusters.[56] $k_{i\to j}$ is the reaction rate coefficient of the chemical reaction from reactant cluster i to product cluster j. The hydration reaction in **GA**-based clusters can be uncatalyzed or catalyzed by **SA**, **W**, or **A**, as described in our previous study.[34] The nature of hydration reactions occurring in a certain **GA**-based cluster depends on the molecules the cluster contains, and the reaction rate corresponding to the catalyst molecule with the lowest activation free energy barrier has been chosen as the representative rate. (The additional molecules present in the cluster might conceivably also affect the reaction rate which was neglected in the present study.)

The collision rate coefficient $\beta_{i,j}$ between clusters i and j was calculated using hard-sphere collision theory,[58]

$$\beta_{i,j} = \pi(r_i + r_j)^2\sqrt{\frac{8k_BT}{\pi\mu}}, \quad (2)$$

where r_i is the radius of cluster i given by the Multiwfn 3.3.8 program,[53] k_B is the Boltzmann constant, T is the temperature,

and $\mu = m_i m_j/(m_i + m_j)$ is the reduced mass. The cluster radius is half of the sum of the distance between the center of most distant atoms in the cluster given by the Multiwfn 3.3.8 program[53] and the van der Walls radii of these atoms.

Evaporation coefficients, $\gamma_{(i+j)\to i}$, were obtained from the corresponding collision coefficients and the Gibbs free energies of cluster formation using

$$\gamma_{(i+j)\to i} = \beta_{i,j}\frac{p_{ref}}{k_B T}\exp\left(\frac{\Delta G_{i+j} - \Delta G_i - \Delta G_j}{k_B T}\right), \quad (3)$$

where p_{ref} is the reference pressure (in this case 1 atm) at which the formation free energies were calculated and ΔG_{i+j} is the Gibbs free energy of formation of cluster $i+j$ from monomers i and j.

The forward and reverse reaction rate coefficients of the chemical reaction were calculated according to the corresponding forward and reverse Gibbs free energy barrier using Eyring's equation as[59]

$$k = \frac{k_B T}{h} e^{-\frac{\Delta G^{\ddagger}}{RT}}, \quad (4)$$

where k_B is Boltzmann's constant, h is Planck's constant, and $\Delta G^{\ddagger}$ is the Gibbs free energy of activation. The Gibbs free energy barrier and rate constants of the forward and reverse reactions are shown in Tables S1 and S2 of the supplementary material.[34]

In addition, the tunneling effects could enhance the rate of the chemical reaction involving hydrogen atom transfer especially at low temperatures.[60] Thus, the effect of tunneling on the hydration reaction is considered to correct the corresponding reaction rate constant through the Wigner tunneling correction by a factor $\Gamma(T)$ as

$$\Gamma(T) = 1 + \frac{1}{24}\left(\frac{h\nu^{\mp}}{k_B T}\right)^2, \quad (5)$$

where h is Planck's constant, k_B is Boltzmann's constant, T is the temperature, and $\nu^{\mp}$ is the imaginary frequency of the transition state.

Then, the Wigner tunneling factor corrected forward and reverse reaction rate coefficients ($k_{i\to j}$, $k_{j\to i}$) of the chemical reaction can be calculated by the tunneling factor as

$$k_{\mathrm{cor}} = \Gamma k. \quad (6)$$

The data of $\Gamma(T)$ of all hydration reactions in the present study at different temperatures (220, 240, 260, 280 and 300 K) are listed in Table S3 of the supplementary material. It indicates that the maximum value of the $\Gamma(T)$ among all the reactions of the present study is 4.34 (the uncatalyzed hydration reaction) at 220 K, which indicates that the tunneling effect has relatively small influence on the present study. The final hydration reaction rate coefficients are still corrected by the Wigner tunneling factor (Table S4 of the supplementary material) to make the results more accurate.

Atmospheric clusters of hygroscopic species are almost invariably hydrated because the concentration of water in the atmosphere is much larger than that of other condensable species. All the hydrated clusters in the studied system with a relative population of higher than 5% are considered. Furthermore, the effective collision and evaporation coefficients of clusters need to be computed as a weighted average over the hydrate distributions to get the effective collision and evaporation coefficients.

The hydrate distributions for a cluster **C** were calculated as[61]

$$f(\mathbf{CW}_i) = \frac{[\mathbf{CW}_i]}{\sum_{j=0}^{j_{\max}}[\mathbf{CW}_j]}, \quad (7)$$

where **C** is a dry molecule or cluster other than water, **W** is water, $\mathbf{CW}_i$ is the cluster consisting of **C** and i water molecules, and $[\mathbf{CW}_i]$ is the concentration of cluster $\mathbf{CW}_i$,

$$\frac{[\mathbf{CW}_i]}{[\mathbf{C}]} = \left([\mathbf{W}]\frac{k_B T}{p_{ref}}\right)^i \exp\left(\frac{\Delta G(\mathbf{C}) - \Delta G(\mathbf{CW}_i)}{k_B T}\right), \quad (8)$$

where $[\mathbf{W}]$ is the concentration of water vapor and p_{ref} is the reference pressure (in this case 1 atm) at which the Gibbs free energies are calculated.

The effective collision coefficients were calculated as

$$\beta_{eff}(\mathbf{C}+\mathbf{D}) = \sum_{i=0}^{i_{\max}}\sum_{j=0}^{j_{\max}}\beta\left(\mathbf{CW}_i + \mathbf{DW}_j\right)f(\mathbf{CW}_i)f\left(\mathbf{DW}_j\right), \quad (9)$$

the effective evaporation coefficients similarly as

$$\gamma_{eff}(\mathbf{CD}\to\mathbf{C}+\mathbf{D}) = \sum_{i=0}^{i_{\max}}\sum_{j=0}^{j_{\max}}\gamma\left(\mathbf{CDW}_{i+j}\to\mathbf{CW}_i + \mathbf{DW}_j\right)f\left(\mathbf{CDW}_{i+j}\right), \quad (10)$$

and the reaction rate coefficient as

$$k_{eff}(\mathbf{C}\to\mathbf{D}) = \sum_{i=1}^{i_{\max}} k_{\mathrm{cor}}(\mathbf{CW}_i\to\mathbf{DW}_{i-1})f(\mathbf{CW}_i). \quad (11)$$

Thus, when considering the presence of water, the birth-death equations can be written as

$$\frac{dc_i}{dt} = \frac{1}{2}\sum_{j<i}\beta_{eff\,j,(i-j)}c_j c_{(i-j)} + \sum_j \gamma_{eff\,(i+j)\to i}c_{i+j} - \sum_j \beta_{eff\,i,j}c_i c_j - \frac{1}{2}\sum_{j<i}\gamma_{eff\,i\to j}c_i + \sum_j k_{eff\,j\to i}c_j - \sum_j k_{eff\,i\to j}c_i + Q_i - S_i. \quad (12)$$

The concentration of sulfuric acid **SA**, **A**, and **GA** is set in the range of 1.0×10^4–1.0×10^8 molecules cm^{-3},[62–65] 1.0×10^7–1.0×10^{11} molecules cm^{-3},[62] and 1.0×10^7–1.0×10^{11} molecules cm^{-3},[32,66–68] respectively, which are relevant to the corresponding common atmospheric concentration. The water vapour concentration was adjusted depending on the temperature according to the study on the saturation vapor pressure from the work of Arnold Wexler.[69] The model runs were performed in the temperature range from 220 K to 300 K, representing the range from the ground level to the upper free troposphere, and RH ranged from 0% to 100%.

The boundary conditions require the outgrowing clusters to have a favorable composition so that the clusters leaving the studied size range are stable enough not to evaporate back immediately. The $(\mathbf{SA})_3\cdot\mathbf{A}_1$ cluster, with a maximum evaporation rate coefficient of 55 s^{-1} at 300 K, is relatively stable enough to resist evaporation (the evaporation rate coefficients of clusters are shown in Table S5 of the supplementary material). Thus, the boundary condition was set to be the $(\mathbf{SA})_3\cdot\mathbf{A}_1$

cluster (see Sec. II in the supplementary material for details). It should be noted that using this relatively small cluster as a boundary condition might overestimate absolute NPF rates, but it is probably sufficient for probing the relative effect of **GA/GW** on the cluster formation rate which is the purpose of this study.

III. RESULTS AND DISCUSSION

The clustering process of **GA**, involving the hydration reaction, includes two kinds of processes (Fig. 1). Process 1 is the formation of **GA**-**SA**-**A** containing clusters involving only collision and evaporation steps (without chemical reactions). Process 2 involves not only the collision and evaporation of **GW**-**SA**-**A** containing clusters but also the hydration reactions of **GA**-based clusters to form **GW**-based clusters.

A. Structure and thermodynamic analysis

The clustering process of **GA** considering the hydration reaction involves 35 different unhydrated and hydrated clusters (Figs. S1–S6 of the supplementary material). The Cartesian coordinates of all clusters are listed in Tables S6–S83 of the supplementary material. The atoms in molecules (AIM) analyses were performed to search the bond critical points (BCPs) and ring critical points (RCPs) and to calculate electron density ρ and Laplacian $\nabla^2\rho$ at the BCPs (Table S84 of the supplementary material). The AIM plots of the clusters without water molecules are shown in Fig. S7 of the supplementary material. All these AIM results affirm the existence of intermolecular interactions in clusters. Moreover, the values of ρ and $\nabla^2\rho$ at these BCPs range from 0.0115 to 0.0927 a.u. and 0.0288 to 0.1815 a.u., respectively. Most of these values are larger than the critical threshold limits for the formation of hydrogen bonds suggested in the literature [0.002–0.040 a.u. and 0.014–0.139 a.u. for ρ (BCP) and $\nabla^2\rho$ (BCP), respectively].[70,71] These values of ρ and $\nabla^2\rho$ thus indicate quite strong hydrogen bond interactions. In addition, there is a large cluster rearrangement after the chemical reaction. The **GA** molecule binds preferentially to the periphery of the cluster (linear), almost solely by the interaction between its carboxyl group and sulfuric acid. After the reaction, both of the carboxyl group and the hydroxyl groups of **GW** can interact with all the other clustering constituents inside the cluster (cage-like).

From the Gibbs free energies of formation of clusters (Fig. S8 of the supplementary material), it can be seen that the clusters based on $(\mathbf{GA})_1\cdot(\mathbf{SA})_1$ and $(\mathbf{GA})_1\cdot(\mathbf{SA})_2$ are more stable than their corresponding **GW**-based analogs. By contrast, the hydrated clusters based on $(\mathbf{GW})_1\cdot(\mathbf{SA})_1\cdot\mathbf{A}_1$ are much more stable than their corresponding **GA**-based analogs at different temperatures.

B. Relative hydration population

GA and **GW** are both water soluble organics, and they can influence the hydrate distribution of clusters. The relative hydration population of clusters with varying numbers of water molecules at different relative humidities (20%, 40%, 60%, and 100%) and a moderate temperature of 260 K are shown in Fig. 2. The influence of **GA** and **GW** on the relative hydration population of clusters is different. The addition of **GA** to the $(\mathbf{SA})_1\cdot\mathbf{A}_1$ cluster reduces the relative population of clusters with four water molecules, enhancing that of clusters without water molecules, while the addition of **GA** on the $(\mathbf{SA})_2$ cluster reduces the relative population of clusters with three water molecules, making the population more even. Thus, the addition of **GA** reduces the ability of $(\mathbf{SA})_1\cdot\mathbf{A}_1$ and $(\mathbf{SA})_2$ clusters to bind more water molecules. However, addition of **GW** to the $(\mathbf{SA})_1\cdot\mathbf{A}_1$ cluster enhances the relative population of clusters with four water molecules, reducing that of clusters without water molecules, while the addition of **GW** on the $(\mathbf{SA})_2$ cluster enhances the relative population of clusters with five water molecules. Thus, the addition of **GW** enhances the ability of $(\mathbf{SA})_1\cdot\mathbf{A}_1$ and $(\mathbf{SA})_2$ clusters to bind more water

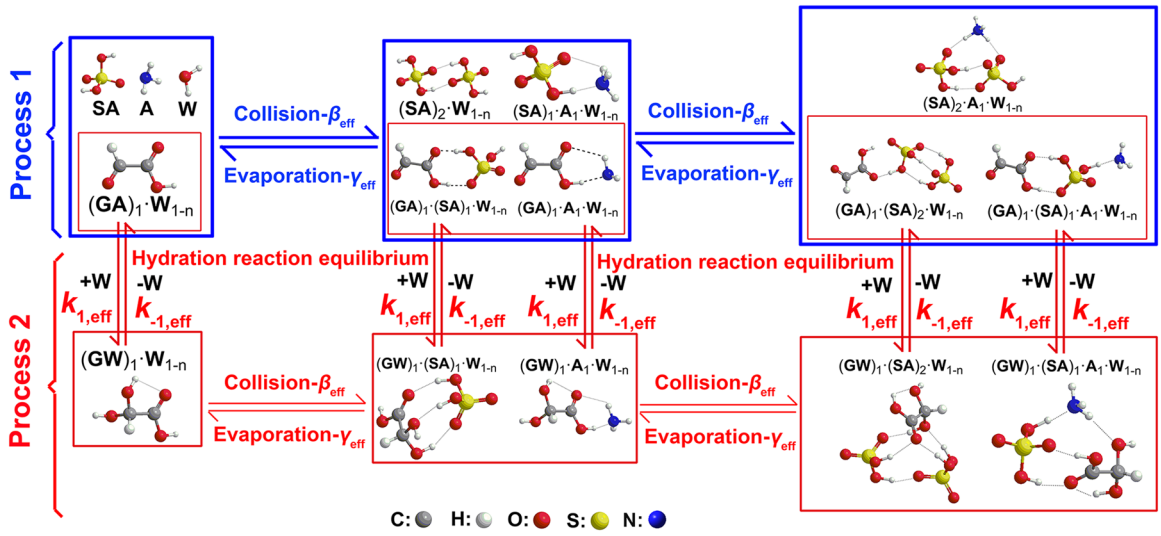

FIG. 1. Modeled clustering processes involving the hydration reaction of **GA** and **GA/GW**-based clusters. Process 1 (formation of **GA**-based clusters) and process 2 (formation of **GW**-based clusters) are shown in the blue and red line frame, respectively. For simplicity, water molecules in the cluster structures are not shown.

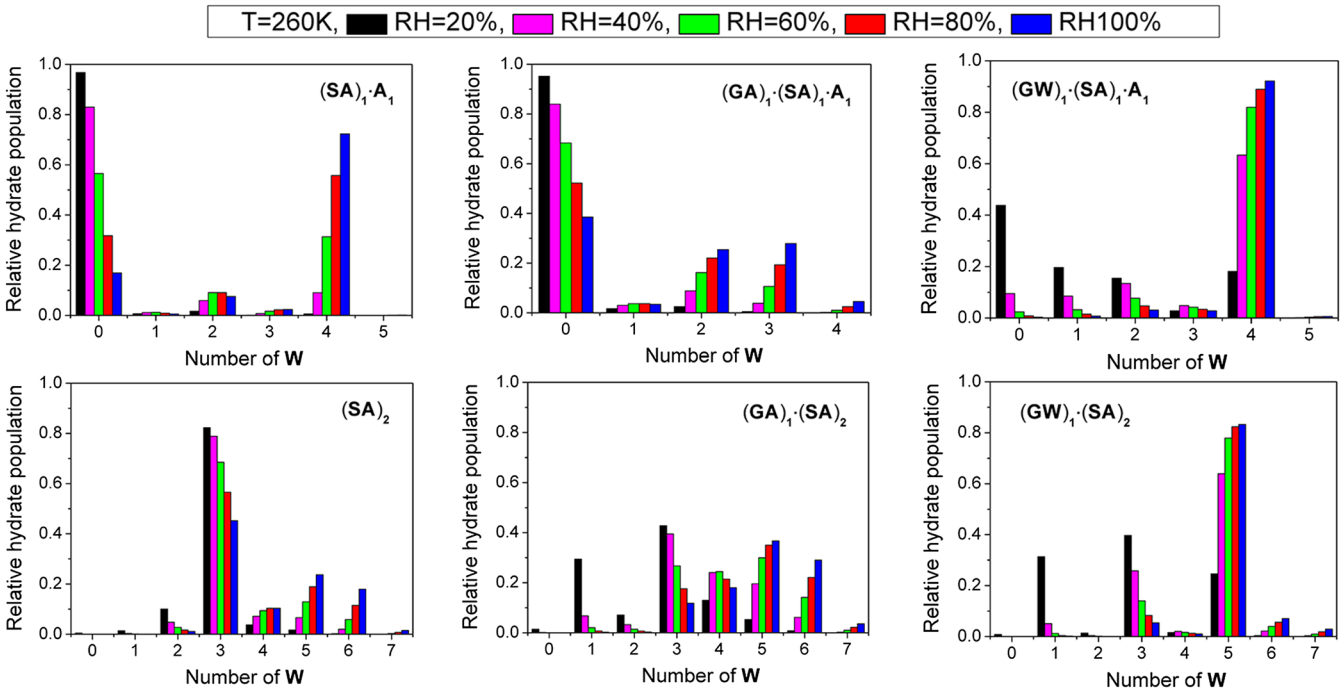

FIG. 2. Hydrate distributions of selected clusters at varying relative humidities at 260 K.

molecules. This difference between the influence of **GA** and **GW** on the cluster hydration population can be explained from the structure characteristic and thermodynamic stability of the corresponding clusters. Two kinds of groups (carboxyl group and hydroxyl group) of **GW** can form hydrogen bonds, whereas only one group (carboxyl group) of **GA** participates in the hydrogen bond formation in the stable structures of clusters (Figs. S1–S6 of the supplementary material). Moreover, the Gibbs free energies of formation of the hydrated clusters involving **GW** with relatively high population are more negative than those involving **GA**.

Based on this result, the hydration reaction products of oxocarboxylic acids can be expected to drastically increase the hygroscopicity of clusters.

C. The realistic hydration reaction conversion ratio of GA-based clusters

The hydration reaction in **GA**-based clusters can be uncatalyzed or catalyzed by **SA**, **W** or **A**, as described in our previous study.[34] Which kind of hydration reaction occurs in a certain **GA**-based cluster depends on what kinds of molecules the cluster contains. Here, we assume that the reaction is always catalyzed by the most effective (lowest activation free energy barrier) catalyst present. In addition, clusters with different number of water molecules may have different hydration reaction pathways available. For example, no hydration reaction is possible for the $(\mathbf{GA})_1\cdot(\mathbf{SA})_1$ cluster, but the **SA** catalyzed hydration reaction can occur in the $(\mathbf{GA})_1\cdot(\mathbf{SA})_1\cdot\mathbf{W}_1$ cluster. Therefore, two factors should be considered to calculate the realistic hydration reaction conversion ratio of **GA**-based clusters: one is the most effective catalysis mechanism and the other is the relative population of the corresponding cluster. Thus, the rate constants corresponding to the catalyst with the lowest activation free energy are weighted by the hydrate distribution. The **GW**-based clusters with i molecules in Fig. 3 can be formed by the collision of the smaller **GW**-based clusters containing i-1 molecules and the evaporation of the bigger **GW**-based clusters containing i + 1 molecules. In addition, they can be formed directly from the hydration reaction of **GA**-based clusters with i + 1 molecules.

The hydration conversion ratio is one of the most important factors determining whether the hydration reaction should be considered in modeling NPF. The hydration reaction occurs either via collision of the two reactant molecules (**GA** and **W**) or in the clusters. Depending on the cluster composition, several different catalyzed processes may be possible.[34] The pathway with the lowest activation free energy barrier is always included in our process model (Fig. 4).

The hydration conversion ratio ($X_{\mathbf{GA}}$) of **GA** in the studied system is defined as

$$X_{\mathbf{GA}}(\%) = \frac{\sum\left[(\mathbf{GW})_1\cdot(\mathbf{SA})_y\cdot\mathbf{A}_z\cdot\mathbf{W}_n\right]}{\sum\left(\left[\left[(\mathbf{GA})_1\cdot(\mathbf{SA})_y\cdot\mathbf{A}_z\cdot\mathbf{W}_n\right]+\left[(\mathbf{GW})_1\cdot(\mathbf{SA})_y\cdot\mathbf{A}_z\cdot\mathbf{W}_n\right]\right]\right)}\times 100, \tag{13}$$

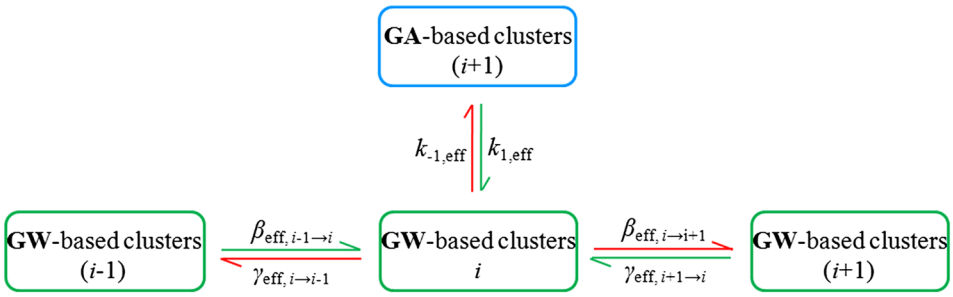

FIG. 3. The source (shown as green arrows) and sink (shown as red arrows) of **GW**-based clusters. Index i indicates the number of the molecules in the cluster. The hydrate distribution has been considered in the effective collision rates β_{eff}, evaporation rates γ_{eff}, and reaction rates k_{eff}. k_{eff} corresponds to the most effective catalyst for the hydration reaction, the nature of which depends on the composition of the cluster.

where $[(\mathbf{GA/GW})_1\cdot(\mathbf{SA})_y\cdot\mathbf{A}_z\cdot\mathbf{W}_n]$ is the concentration of **GA/GW**-based clusters (or, for $y=0$, $z=0$, and $n=0$, **GA/GW** monomers). The denominator represents the sum of all **GA** or **GW** containing clusters (and monomers) in the system, and the numerator represents the numbers of clusters where **GA** has been converted to **GW**. We have modeled the conversion ratio $X_{\mathbf{GA}}$ under different atmospheric conditions (different conditions as shown in Fig. 5 are the chosen so that they correspond to the range of values in the atmosphere). The detailed values of the conversion ratios in different conditions are given in Tables S85 and S86 of the supplementary material.

Figure 5 shows that under most atmospherically relevant conditions, the ammonia (**A**) concentration has no effect on the conversion ratio ($X_{\mathbf{GA}}$), while the RH has a moderate effect. The surprisingly weak RH dependence is caused by a "saturation" of the water-catalyzed pathway already at fairly low RH values. By contrast, $X_{\mathbf{GA}}$ clearly increases with decreasing temperature [Fig. 5(a)] and increases with increasing sulfuric acid (**SA**) concentration [Fig. 5(b)]. That is due to the fact that sulfuric acid catalyzes this reaction much more effectively than ammonia or water.[34] $X_{\mathbf{GA}}$ is more than 50% when **SA** concentration is more than 1.0×10^6 molecules cm^{-3} and can reach up to 85% when the concentration of **SA** is about 1.0×10^7 molecules cm^{-3} [Fig. 5(b)]. The relatively high conversion ratio could significantly affect the relative abundances of oxocarboxylic acids and their corresponding geminal diols and thus NPF, especially in the regions where **SA** is abundant, such as the polluted regions and coastal areas.

D. Cluster formation rate

A suitable measure for the enhancement of the cluster formation rate (J) by **GA** and its hydration reaction product (**GW**) is the comparison of the cluster formation rate involving both **GA** and **GW** with that of **SA**-**A**-based clusters under similar conditions, i.e.,

$$r_1 = \frac{J([\mathbf{GA}+\mathbf{GW}]=x,[\mathbf{SA}]=y,[\mathbf{A}]=z)}{J([\mathbf{GA}]=0,[\mathbf{SA}]=y,[\mathbf{A}]=z)}, \quad (14)$$

where r_1 is the enhancement factor, $J[(\mathbf{GA}+\mathbf{GW})=x]$, $[\mathbf{SA}=y]$, $(\mathbf{A})=z]$ represents the formation rate of $(\mathbf{GA/GW})_x\cdot(\mathbf{SA})\cdot_y\mathbf{A}_z$ clusters with variable numbers of water molecules (and including the effect of **GA** hydration reactions) and $J[(\mathbf{GA})=0$, $(\mathbf{SA})=x$, $(\mathbf{A})=y]$ represents the formation rate of the corresponding clusters without **GA** or **GW**.

As shown in Figs. 6(a)–6(c), the enhancement factor r_1 is greater than 1, which indicates that **GA** can enhance the **SA**-**A**-based cluster formation rate. r_1 increases with the increase of **GA** concentrations but only becomes significant when the temperature is lowered to 220 K. Thus, the influence of relative humidity, sulfuric acid (**SA**) concentration, and ammonia (**A**)

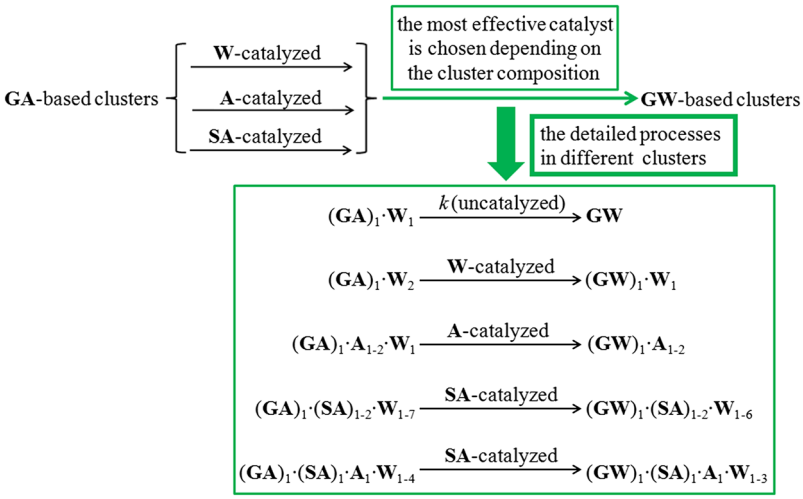

FIG. 4. Detailed information of the hydration reaction in clusters of the studied system.

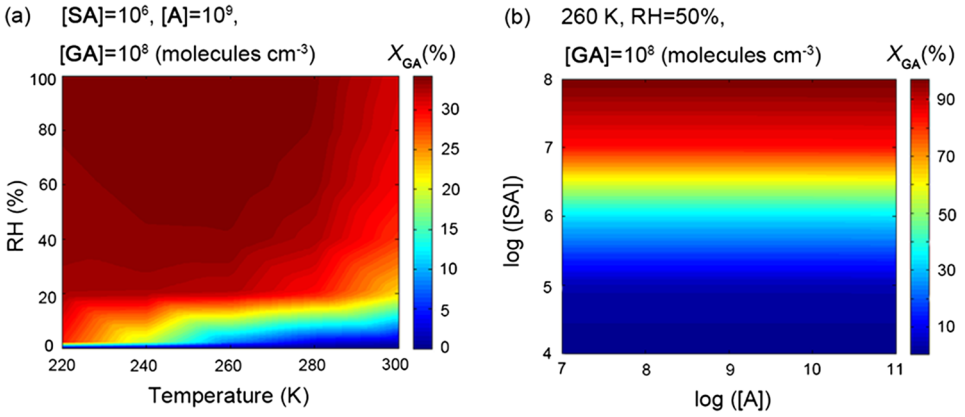

FIG. 5. The conversion ratio, $X_{\mathbf{GA}}$ (%), of glyoxylic acid (**GA**) hydration forming its geminal diol (**GW**) at varying (a) temperatures (K) and RHs (%) and (b) base-10 logarithm of the concentrations (molecules cm^{-3}) of **A** and **SA**. The color scales are shown on the right.

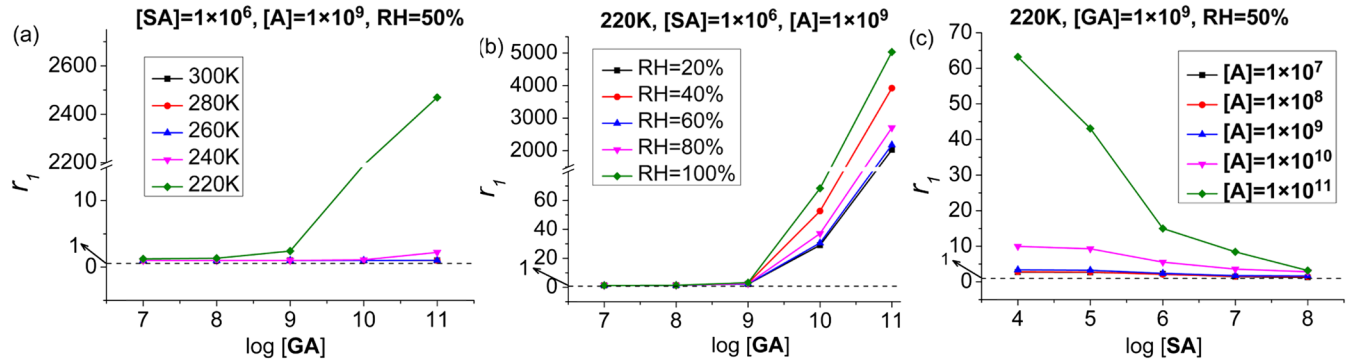

FIG. 6. Enhancement of the **SA**-**A**-**W** cluster formation rate due to **GA** and **GW** as a function of the conditions (concentrations, molecules cm^{-3}) [Eq. (14)].

concentration on the cluster formation rate was studied at 220 K. The enhancement is relatively large at high RH, low **SA** concentrations, and high **A** concentrations. The enhancement factor exceeds 10 with the **SA** concentration lower than 1.0×10^6 molecules cm^{-3} and a high **A** concentration of 1.0×10^{11} molecules cm^{-3}, at which the absolute formation rate of **GA**-**SA**-**A**-based clusters is as high as 2.77×10^4 cm^{-3} s^{-1} (the absolute formation rates of **GA**-**SA**-**A**-based clusters at different temperatures, RHs, and concentrations of **GA**, **SA**, and **A** are listed in Tables S87–S89 of the supplementary material). When the **SA** concentration is low, and the **A** concentration high, there will be enough **A** to cluster with **GA** and **GW** despite the stronger binding between **SA** and **A** compared to **GA**/**GW** and **A**.

To assess the significance of the hydration reaction of **GA**, we compared the cluster formation with **GA** present, but both with and without hydration reactions (Fig. 7). A suitable measure for the effect of the hydration reaction is the ratio of formation rates in the case where the hydration reaction of **GA** to form **GW** is allowed to the rate in the case when this reaction is not occurring,

$$r_2 = \frac{J([\mathbf{GA}+\mathbf{GW}] = x, [\mathbf{SA}] = y, [\mathbf{A}] = z)}{J([\mathbf{GA}] = x, [\mathbf{SA}] = y, [\mathbf{A}] = z)}, \qquad (15)$$

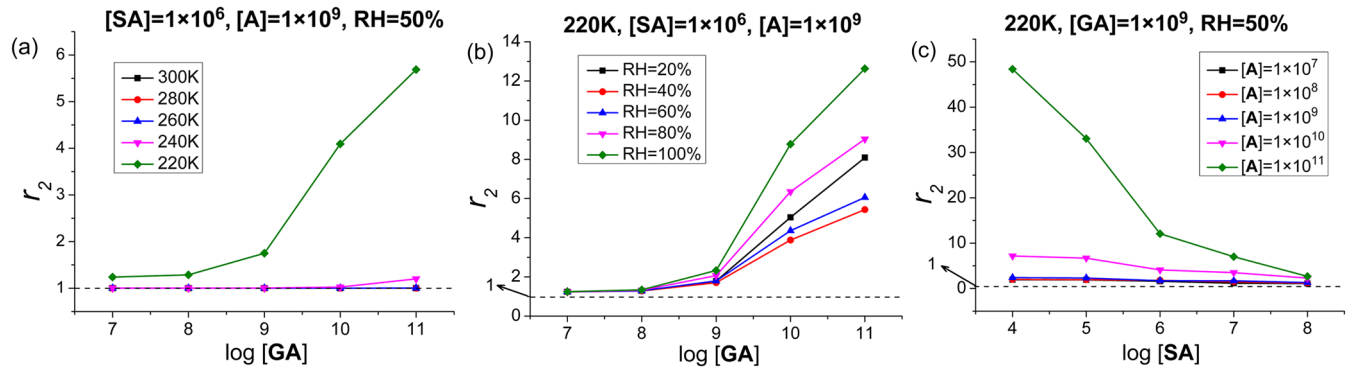

FIG. 7. Cluster formation rate involving **GA** and its hydration reaction relative to that involving **GA** but not its hydration reaction [Eq. (15)].

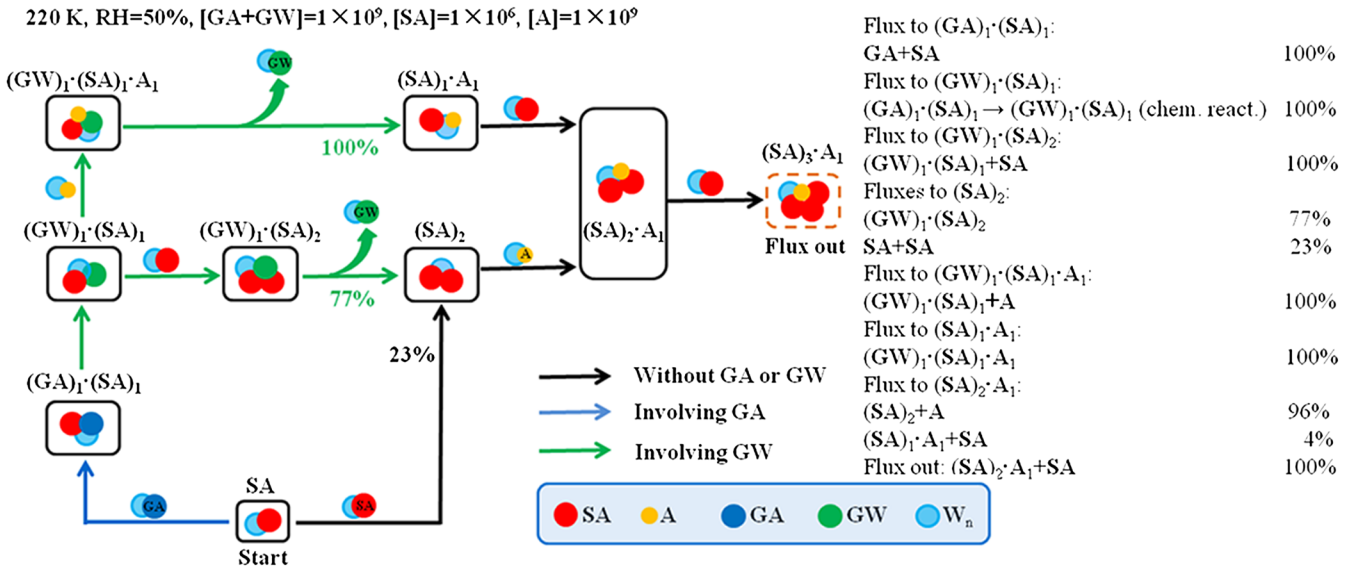

FIG. 8. Main cluster formation pathways considering the hydration reaction of **GA** forming **GW** are represented by arrows. Relative amounts of clusters formed via dominating growth pathways are indicated in the side table.

where J [(**GA** = x, (**SA**) = y, (**A**) = z)] indicates the cluster formation rate in a system involving **GA** but not allowing the hydration reaction.

The common trend is that r_2 increases with an increase of **GA** concentrations, but is not significant until the temperature is lowered to 220 K [Fig. 7(a)]. Thus, the influence of relative humidity, sulfuric acid (**SA**) concentration, and ammonia (**A**) concentration on the cluster formation rate was studied at 220 K. The effect of hydration reactions on NPF is more significant at high RH, low sulfuric acid (**SA**) concentration, and high ammonia (**A**) concentration. The likely explanation for this is that when the **SA** concentration is low and the **A** concentration high, there will be enough **A** for **GA** and **GW** regardless of the stronger combination between **SA** and **A**. This makes the competition between **GA** and **GW** more pronounced, enhancing the ratio between cluster formation rates with hydration switched "on" and "off." Thus, both the effect of **GA** and its hydration reaction are most significant in cold, humid, and relatively clean environments with little sulfuric acid or agricultural regions polluted with ammonia.

E. Cluster formation pathway

The main cluster formation pathways involving the hydration reaction of **GA** to form **GW** have been further studied at 220 K (Fig. 8). The flux through the system proceeds principally via two clustering mechanisms: one involves pure **SA**-**A**-clusters and the other involves one **GA** or **GW** molecule in addition to **SA** and **A**. The clusters grow out of the size region studied through the addition of sulfuric acid to $(\mathbf{SA})_2\cdot\mathbf{A}_1$ clusters. **GA**-based clusters easily form **GW**-based clusters through hydration reactions, for example, converting $(\mathbf{GA})_1\cdot(\mathbf{SA})_1\cdot\mathbf{W}_n$ to $(\mathbf{GW})_1\cdot(\mathbf{SA})_1\cdot\mathbf{W}_{n-1}$. Though **GA** and **GW** evaporate easily from clusters from the point of view of the cluster stability, the contribution of **GW** to the formation of $(\mathbf{SA})_2$ or $(\mathbf{SA})_1\cdot\mathbf{A}_1$ clusters can still reach up to 77% and 100%, respectively, due to the high concentration of **GA** and the high hydration conversion ratio combined with the thermodynamic stability. At the conditions corresponding to high R values, nearly 100% of the $(\mathbf{SA})_2\cdot(\mathbf{A})_1$ clusters are formed via $(\mathbf{GW})_1\cdot(\mathbf{SA})_1\cdot\mathbf{A}_1$ clusters (Fig. S9 of the supplementary material). Thus, the contribution of **GA** to **SA**-**A** NPF is potentially of great significance especially in the regions where the hydration conversion ratio is large.

IV. CONCLUSIONS

The clustering mechanism involving the hydration reaction of glyoxylic acid, as a representative example of oxocarboxylic acids, has been studied using the density functional theory combined with the Atmospheric Cluster Dynamic Code. The hydration reaction induces the difference in cluster structures, and the hydration reaction products of glyoxylic acid can drastically increase the hygroscopicity of clusters. Under atmospheric conditions, the total hydration reaction conversion ratio of glyoxylic acid to its product (2,2-dihydroxyacetic acid) in both gas phase and clusters can be up to 85%, and the product can further participate in the clustering process. Thus, it can be speculated that the relatively high conversion ratio could significantly affect the relative abundances of oxocarboxylic acids and their corresponding geminal diols and thus NPF.

Neglecting the hydration reaction can thus induce a significant error in cluster formation rates and pathways, especially at relatively low temperatures. In addition, the evaporation rates of larger oxocarboxylic acids (and especially their germinal diols) can be expected to be lower due to more H-bonding groups and higher molecular weights. They are thus likely to participate in the cluster formation also at higher temperatures. Thus, the hydration reaction of oxocarboxylic acids in the clustering process may be of greater importance in the atmosphere. A more general inference from the present study is that the hydration reactions of oxocarboxylic acids catalyzed by clustering with sulfuric acid and ammonia can increase both

the hygroscopicity and stability of clusters and thus contribute to NPF. The present study can provide a clearer picture of the effect mechanism of oxocarboxylic acids in NPF and indicates the prospect of the nucleation process involving chemical reactions, which has significant implications for the improvement of the atmospheric models.

SUPPLEMENTARY MATERIAL

See supplementary material for the Gibbs free energy barrier (kcal/mol) and the reaction rate constants (Ref. 34), the Wigner tunneling correction factor and the tunneling effect factor corrected reaction rate constants for hydration reactions of **GA** with **W**: (a) uncatalyzed, (b) catalyzed by **W**, (c) catalyzed by **SA**, and (d) catalyzed by **A** at varying temperatures ranging from 220 K to 300 K, evaporation rate coefficients of clusters, Cartesian coordinates of all clusters, AIM topological parameters for the stable clusters, the realistic hydration reaction conversion ratio ($X_{\mathbf{GA}}$), formation rates of clusters, the most stable configuration of the studied clusters, the AIM plots of the unhydrated clusters, Gibbs free energies of formation of clusters, the main cluster formation pathways considering the hydration reaction of **GA** forming **GW**, details for the boundary conditions, and complete Gaussian 09 reference (Ref. 52).

ACKNOWLEDGMENTS

The authors thank the Chinese National Natural Science Foundation (Nos. 21373025, 91544223, 91544227, 21473010, and 21673018) and the "Fundamental Research Funds for the Central Universities" for the support of this research. O. Kupiainen-Määttä thanks the European Research Council (Grant No. 257360-MOCAPAF). T.K. thanks the Academy of Finland for funding. H.V. thanks the European Research Council (Grant No. 692891-DAMOCLES) and the University of Helsinki, Faculty of Science ATMATH project for funding.

[1] K. K. Ding, X. T. Kong, J. P. Wang, L. P. Lu, W. F. Zhou, T. J. Zhan, C. L. Zhang, and S. L. Zhuang, Environ. Sci. Technol. Lett. **51**, 6452 (2017).
[2] A. G. Rincón, M. I. Guzmán, M. R. Hoffmann, and A. J. Colussi, J. Phys. Chem. A **113**, 10512 (2009).
[3] C. L. Heald, D. J. Jacob, R. J. Park, L. M. Russell, B. J. Huebert, J. H. Seinfeld, H. Liao, and R. J. Weber, Geophys. Res. Lett. **32**, L18809, https://doi.org/10.1029/2005gl023831 (2005).
[4] R. Volkamer, J. L. Jimenez, F. S. Martini, K. Dzepina, Q. Zhang, D. Salcedo, L. T. Molina, D. R. Worsnop, and M. J. Molina, Geophys. Res. Lett. **33**, L17811, https://doi.org/10.1029/2006gl026899 (2006).
[5] R. Y. Zhang, I. Suh, J. Zhao, D. Zhang, E. C. Fortner, X. X. Tie, L. T. Molina, and M. J. Molina, Science **304**, 1487 (2004).
[6] R. Y. Zhang, A. Khalizov, L. Wang, M. Hu, and W. Xu, Chem. Rev. **112**, 1957 (2012).
[7] H. L. Zhao, Q. Zhang, and L. Du, RSC Adv. **6**, 71733 (2016).
[8] Q. Zhang and L. Du, Comput. Theor. Chem. **1078**, 123 (2016).
[9] I. K. Ortega, N. M. Donahue, T. Kurtén, M. Kulmala, C. Focsa, and H. Vehkamäki, J. Phys. Chem. A **120**, 1452 (2016).
[10] J. Elm, N. Myllys, T. Olenius, R. Halonen, T. Kurtén, and H. Vehkamäki, Phys. Chem. Chem. Phys. **19**, 4877 (2017).
[11] H. B. Xie, J. Elm, R. Halonen, N. Myllys, T. Kurtén, M. Kunlmala, and H. Vehkamäki, Environ. Sci. Technol. **51**, 8422 (2017).
[12] C. Chirs, Nature **533**, 478 (2016).
[13] S. Li, K. Qu, H. Zhao, L. Ding, and L. Du, Chem. Phys. **472**, 198 (2016).
[14] H. L. Zhao, S. S. Tang, S. Y. Li, L. Ding, and L. Du, Struct. Chem. **27**, 1241 (2016).
[15] J. Elm, M. Passananti, T. Kurtén, and H. Vehkamäki, J. Phys. Chem. A **121**, 6155 (2017).
[16] S. Guo, M. Hu, M. L. Zamora, J. F. Peng, D. J. Shang, J. Zheng, Z. F. Du, Z. J. Wu, M. Shao, L. M. Zeng, M. J. Molina, and R. Y. Zhang, Proc. Natl. Acad. Sci. U. S. A. **111**, 17373 (2014).
[17] N. Zhao, Q. Z. Zhang, and W. X. Wang, Sci. Total Environ. **563-564**, 1008 (2016).
[18] J. Dang, X. L. Shi, Q. Z. Zhang, and W. X. Wang, Sci. Total Environ. **517**, 1 (2015).
[19] X. W. Wang, B. Jing, F. Tan, J. B. Ma, Y. H. Zhang, and M. F. Ge, Atmos. Chem. Phys. **17**, 12797 (2017).
[20] V. Hirvonen, N. Myllys, T. Kurtén, and J. Elm, J. Phys. Chem. A **122**, 1771 (2018).
[21] H. B. Xie, F. F. Ma, Q. Yu, N. He, and J. W. Chen, J. Phys. Chem. A **121**, 1657 (2017).
[22] J. Liu, S. Fang, Z. Wang, W. Yi, F.-M. Tao, and J. Y. Liu, Environ. Sci. Technol. **49**, 13112 (2015).
[23] J. J. Liu, S. Fang, W. Liu, M. Y. Wang, F. M. Tao, and J. Y. Liu, J. Phys. Chem. A **119**, 102 (2015).
[24] X. Shi, R. Zhang, Y. Sun, F. Xu, Q. Zhang, and W. Wang, Phys. Chem. Chem. Phys. **20**, 1005 (2018).
[25] T. Kurtén, J. Elm, N. L. Prisle, K. V. Mikkelsen, C. J. Kampf, E. M. Waxman, and R. Volkamer, J. Phys. Chem. A **119**, 4509 (2015).
[26] M. Shrivastava, C. D. Cappa, J. Fan, A. H. Goldstein, A. B. Guenther, J. L. Jimenez, C. Kuang, A. Laskin, S. T. Martin, N. L. Ng, T. Petaja, J. R. Pierce, P. J. Rasch, P. Roldin, J. H. Seinfeld, J. Shilling, J. N. Smith, J. A. Thornton, R. Volkamer, J. Wang, D. R. Worsnop, R. A. Zaveri, A. Zelenyuk, and Q. Zhang, Rev. Geophys. **55**, 509, https://doi.org/10.1002/2016rg000540 (2017).
[27] K. L. Plath, J. L. Axson, G. C. Nelson, K. Takahashi, R. T. Skodje, and V. Vaidaa, React. Kinet. Catal. Lett. **96**, 209 (2009).
[28] J. L. Axson, K. Takahashi, D. O. D. Haan, and V. Vaida, Proc. Natl. Acad. Sci. U. S. A. **107**, 6687 (2010).
[29] M. K. Hazra, J. S. Francisco, and A. Sinha, J. Phys. Chem. A **117**, 11704 (2013).
[30] M. K. Hazra, J. S. Francisco, and A. Sinha, J. Phys. Chem. A **118**, 4095 (2014).
[31] R. J. Weber, J. J. Marti, P. H. McMurry, F. L. Elsele, D. J. Tanner, and A. Jefferson, Chem. Eng. Commun. **151**, 53 (1996).
[32] R. Ortiz, K. Enya, K. Sekiguchi, and K. Sakamoto, Atmos. Environ. **43**, 382 (2009).
[33] G. H. Wang, K. Kawamura, C. L. Cheng, J. J. Li, J. J. Cao, R. J. Zhang, T. Zhang, S. X. Liu, and Z. Z. Zhao, Environ. Sci. Technol. **46**, 4783 (2012).
[34] L. Liu, X. H. Zhang, Z. S. Li, Y. H. Zhang, and M. F. Ge, Chemosphere **186**, 430 (2017).
[35] M. J. McGrath, T. Olenius, I. K. Ortega, V. Loukonen, P. Paasonen, T. Kurtén, M. Kulmala, and H. Vehkamäki, Atmos. Chem. Phys. **12**, 2345 (2012).
[36] H. Henschel, J. C. A. Navarro, T. Yli-Juuti, O. Kupiainen-Määttä, T. Olenius, I. K. Ortega, S. L. Clegg, T. Kurtén, I. Riipinen, and H. Vehkamäki, J. Phys. Chem. A **118**, 2599 (2014).
[37] J. Zhang and M. Dolg, Phys. Chem. Chem. Phys. **17**, 24173 (2015).
[38] J. Zhang and M. Dolg, Phys. Chem. Chem. Phys. **18**, 3003 (2016).
[39] A. D. MacKerell, Jr., D. Bashford, M. Bellott, J. R. L. Dunbrack, J. D. Evanseck, M. J. Field, S. Fischer, J. Gao, H. Guo, S. Ha, D. Joseph-McCarthy, L. Kuchnir, K. Kuczera, F. T. K. Lau, C. Mattos, S. Michnick, T. Ngo, D. T. Nguyen, B. Prodhom, W. E. Reiher III, B. Roux, M. Schlenkrich, J. C. Smith, R. Stote, J. Straub, M. Watanabe, J. Wiórkiewicz-Kuczera, D. Yin, and M. Karplus, J. Phys. Chem. B **102**, 3586 (1998).
[40] J. J. P. Stewart, J. Mol. Model. **13**, 1173 (2007).
[41] J. J. P. Stewart, J. Mol. Model. **19**, 1 (2013).
[42] J. J. P. Stewart, Stewart Computational Chemistry, Colorado Springs, CO, USA, http://OpenMOPAC.net (2016).
[43] Y. Zhao and D. G. Truhlar, Theor. Chem. Acc. **120**, 215 (2008).
[44] Y. Zhao and D. G. Truhlar, Chem. Phys. Lett. **502**, 1 (2011).
[45] M. J. Frisch, J. A. Pople, and J. S. Binkley, Chem. Phys. Lett. **80**, 3265 (1984).
[46] J. Elm, M. Bilde, and K. V. Mikkelsen, J. Chem. Theory Comput. **8**, 2071 (2012).
[47] J. Elm, M. Bilde, and K. V. Mikkelsen, Phys. Chem. Chem. Phys. **15**, 16442 (2013).
[48] J. Herb, A. B. Nadykto, and F. Q. Yu, Chem. Phys. Lett. **518**, 7 (2011).
[49] A. B. Nadykto, F. Yu, M. V. Jakovleva, J. Herb, and Y. Xu, Entropy **13**, 554 (2011).

[50]A. B. Nadykto, F. Yu, and J. Herb, Atmos. Chem. Phys. **9**, 4031 (2009).
[51]J. Herb, Y. Xu, F. Yu, and A. B. Nadykto, J. Phys. Chem. A **117**, 133 (2013).
[52]M. J. Frisch, G. W. Trucks, and H. B. Schlegel *et al.*, GAUSSIAN 09, Revision A.1, Gaussian, Inc., Wallingford, CT, 2009 (see supplementary material for details).
[53]T. Lu and F. Chen, J. Comput. Chem. **33**, 580 (2012).
[54]T. Olenius, O. Kupiainen-Määttä, I. K. Ortega, T. Kurtén, and H. Vehkamäki, J. Chem. Phys. **139**, 084312 (2013).
[55]L. F. Shampine and M. W. Reichelt, SIAM J. Sci. Comput. **18**, 1 (1997).
[56]N. Bork, J. Elm, T. Olenius, and H. Vehkamäki, Atmos. Chem. Phys. **14**, 12023 (2014).
[57]M. Kulmala, M. Dal Maso, J. M. Mäkelä, L. Pirjola, M. Väkevä, P. Aalto, P. Miikkulainen, C. D. Hämeri, and K. O'dowd, Tellus B **53**, 479–490 (2001).
[58]J. H. Seinfel and S. N. Pandis, *Atmospheric Chemistry and Physics: From Air Pollution to Climate Change* (John Wiley & Sons, Inc., New York, 2006).
[59]H. Eyring, J. Chem. Phys. **3**, 107 (1935).
[60]M. Kumar, J. M. Anglada, and J. S. Francisco, J. Phys. Chem. A **121**, 4318–4325 (2017).
[61]T. Kurtén, M. Noppel, H. Vehkamäki, M. Salonen, and M. Kulmala, Boreal Environ. Res. **12**, 431 (2007).
[62]I. Riipinen, S. L. Sihto, M. Kulmala, F. Arnold, M. Dal Maso, W. Birmili, K. Saarnio, K. Teinila, V. M. Kerminen, and A. Laaksonen, Atmos. Chem. Phys. **7**, 1899 (2007).
[63]J. Almeida, S. Schobesberger, A. Kürten, I. K. Ortega, O. Kupiainen-Määttä, A. P. Praplan, A. Adamov, A. Amorim, F. Bianchi, M. Breitenlechner, A. David, J. Dommen, N. M. Donahue, A. Downard, E. Dunne, J. Duplissy, S. Ehrhart, R. C. Flagan, A. Franchin, R. Guida, J. Hakala, A. Hansel, M. Heinritzi, H. Henschel, T. Jokinen, H. Junninen, M. Kajos, J. Kangasluoma, H. Keskinen, A. Kupc, T. Kurtén, A. N. Kvashin, A. Laaksonen, K. Lehtipalo, M. Leiminger, J. Leppä, V. Loukonen, V. Makhmutov, S. Mathot, M. J. McGrath, T. Nieminen, T. Olenius, A. Onnela, T. Petäjä, F. Riccobono, I. Riipinen, M. Rissanen, L. Rondo, T. Ruuskanen, F. D. Santos, N. Sarnela, S. Schallhart, R. Schnitzhofer, J. H. Seinfeld, M. Simon, M. Sipilä, Y. Stozhkov, F. Stratmann, A. Tomé, J. Tröstl, G. Tsagkogeorgas, P. Vaattovaara, Y. Viisanen, A. Virtanen, A. Vrtala, P. E. Wagner, E. Weingartner, H. Wex, C. Williamson, D. Wimmer, P. Ye, T. Yli-Juuti, K. S. Carslaw, M. Kulmala, J. Curtius, U. Baltensperger, D. R. Worsnop, H. Vehkamäki, and J. Kirkby, Nature **502**, 359 (2013).
[64]C. Kuang, P. H. Mcmurry, A. V. Mccormick, and F. L. Elsele, J. Geophys. Res. **113**, D10209, https://doi.org/10.1029/2007jd009253 (2008).
[65]S. Schobesberger, H. Junninen, F. Bianchi, G. Lonn, M. Ehn, K. Lehtipalo, J. Dommen, S. Ehrhart, I. K. Ortega, A. Franchin, T. Nieminena, F. Riccobono, M. Hutterli, J. Duplissy, J. Almeida, A. Amorim, M. Breitenlechner, A. J. Downard, E. M. Dunne, R. C. Flagan, M. Kajos, H. Keskinen, J. Kirkby, A. Kupc, T. K. A. Kürten, A. Laaksonen, S. Mathot, A. Onnela, A. P. Praplan, L. Rondo, F. D. Santos, S. Schallhart, R. Schnitzhofer, M. Sipilä, A. Tomé, H. V. G. Tsagkogeorgas, D. Wimmer, U. Baltensperger, K. S. Carslaw, J. Curtius, A. Hansel, T. Petäjä, M. Kulmala, N. M. Donahue, and D. R. Worsnop, Proc. Natl. Acad. Sci. U. S. A. **110**, 17223 (2013).
[66]B. Graham, O. L. Mayol-Bracero, P. Guyon, G. C. Roberts, S. Decesari, M. C. Facchini, P. Artaxo, W. Maenhaut, P. Köll, and M. O. Andreae, J. Geophys. Res.: Atmos. **107**, 8047, https://doi.org/10.1029/2001JD000336 (2002).
[67]W. Y. Zhao, K. Kawamura, S. Y. Yue, L. F. Wei, H. Ren, Y. Yan, M. Kang, L. J. Li, L. J. Ren, S. Lai, J. Li, Y. L. Sun, Z. F. Wang, and P. Q. Fu, Atmos. Chem. Phys. **18**, 2749 (2018).
[68]K. Kawamura, E. Tachibana, K. Okuzawa, S. G. Aggarwal, Y. Kanaya, and Z. F. Wang, Atmos. Chem. Phys. **13**, 8285 (2013).
[69]A. Wexler, J. Res. Natl. Bur. Stand. **80A**, 775 (1976).
[70]U. Koch and P. L. A. Popelier, J. Phys. Chem. **99**, 9747 (1995).
[71]S. J. Grabowski, J. Phys. Org. Chem. **17**, 18 (2004).